Electronic Supplementary Material (ESI) for Journal of Materials Chemistry B.

Silver Nanoparticles-Assisted Signal Amplification Electrochemiluminescence Biosensor for Highly Sensitive Detection of Mucin 1

Yuping Wei, Yiwen Zhang, Changjie Mao *

Anhui Province Key Laboratory of Chemistry for Inorganic/Organic Hybrid Functionalized Materials, School of Chemistry & Chemical Engineering, Anhui University, hefei230601, PR China

Corresponding Author; E-mail: maochangjie@sina.com; Tel & Fax: +86 551 6386 1260.

Materials.

Zirconium tetrachloride, 1, 2, 4, 5-Benzenetetracarboxylic acid (H_4BTe_4), Terephthalic acid (BDC) and Trifluoroacetic acid (TFA) were obtained from Shanghai Macklin Biochemical Co., Ltd (Shanghai China). Europium nitrate hexahydrate and Pyromellitic acid were bought from Aladdin Reagent Co., Ltd (Shanghai, China). 6-Mercapto-1-hexanol (MCH) was bought from Saen Chemical Technology Co., Ltd (Shanghai, China). N, N-Dimethylformamide, Sodium chloride were purchased from Shanghai Reagent Co. Ltd (Shanghai, China). The DNA oligonucleotides, Tris(2-carboxyethyl)-phosphine (TCEP) and HEPES buffer solution were provided by Shanghai Sangon Biological Engineering Technology Co. Ltd (Shanghai, China). prostate-specific antigen (PSA) acquired from Sigma-Aldrich Co. Ltd (Shanghai, China). Interleukin 6 (IL-6), Urokinase-type plasminogen activator (u-PA), carcinoembryonic (CEA) were provided by Beijing Biosynthesis Biotechnology Co. Ltd (Beijing, China). MUC1 was provided by Shanghai Apeptide Co., Ltd (Shanghai, China). All of the above reagents were analytical pure and without further purification. Phosphate buffer saline (PBS pH=7.4, 10 mM) was consisted of 1.76 mM KH_2PO_4, 10.15 mM Na_2HPO_4, 136.89 mM NaCl and 2.67 mM KCl. TM buffer solution (pH=8) was consisted of 20 mM Tris, 50 mM $MgCl_2$. TE buffer solution contained 10 mM Tris·HCl and 1 mM EDTA. Ultrapure water (18MΩ/cm) was used throughout this work.

The DNA sequences were shown in below:

S1: SH-5′-TGC TGG CAC TAG CGC CAC ATG CGC GTA AGT TGC CAT AGA GGC TAG TGT CTC CCA C-3′

S2: SH-5′-TGG CGC TAG TGC CAG CAA AGA AGG AGG GGC GAC CTA TCA CCT

GTT CAG CCG CGA T-3′

S3: SH-5′-TCT CCA GGC CGC ACG TCT ATA GGT CGC CCC TCC TTC TTG TGG GAG ACA CTA GCC T-3′

S4: 5′-GAC GTG CGG CCT GGA GAA CAT GCG AAC TTA CGC GCA GAA TCG CGG CTG AAC AGG TTT TCC AGG GTA TCC A-3′

MUC1 aptamer: 5′-GCA GTT GAT CCT TTG GAT ACC CTG G-3′

Apparatus.

Scanning electron microscope (SEM, REGULUS8230, HITACHI, Japan). Fourier transform infrared spectrometer (FTIR, NEXUS-870, Nicolet Instrument Co., USA). X-ray polycrystalline diffractometer (XRD, Smartlab 9KW, Rigoku, Japan), X-ray photoelectron spectroscopy (XPS, ES-CALAB 250, Thermo Ltd, USA). The cyclic voltammetry (CV) and ECL were performed on CHI-660D electrochemical workstation (Shanghai Chenhua Instrument, China), MPI-E electrochemiluminescence analyzer (Xi′An Remax Co. Ltd., China) respectively. During the measurements, Ag/AgCl electrode, Pt wire electrode and the modified gold electrode (AuE) were used as reference electrode, auxiliary electrode and working electrode respectively. The voltage of photomultiplier was set as 800V. Electrochemical impedance spectrum (EIS) was carried out on the Auto lab electrochemical analyzer (EcoChemie Co., Netherlands) in 5 mM of $Fe(CN)_6^{3-/4-}$ and 0.1 M of KCl.

Feasibility of the biosensor.

EIS and CV were employed to verify the fabrication of the biosensor. As shown in Fig. S2A, the EIS Nyquist plot contained a semicircular portion and a linear portion, which corresponded to the higher frequency region and lower frequencies, respectively. The semicircular portion reflected the electron transfer restricted process (R_{et}). The bare gold electrode (curve a) showed a tiny semicircle in the EIS Nyquist plot, which indicated good conductivity of the electrode. Following modification of the TDNs on the electrode (curve b), the semicircle increased. As Ag NPs can accelerate the electron transfer rate, the semicircle diameter diminished in curve c. The biomacromolecule prevented the transformation of electrons on the electrode. Hence, when MCH (curve d) and DNA-Eu@MOF (curve e), were successfully assembled on the electrode, the impedance increased

continuously and significantly. When the modified electrode was incubated with MUC1 solution, the resistance value decreased markedly (curve f), as the specific binding of MUC1 and aptamer caused the DNA-Eu@MOF to detach from the electrode, and the degree of electron transfer inhibition on the electrode surface was then reduced.

The CV responses of different modified electrodes are shown in Fig. S2B. A pair of well-defined current peaks of $[Fe(CN)_6]^{3-/4-}$ were obtained for the bare gold electrode (curve a). Corresponding to the impedance, the CV response decreased when the electrode was modified by TDNs (curve b). The CV response was restored due to the growth of Ag NPs (curve c). Following modification with MCH (curve d) and DNA-Eu@MOF (curve e), the CV response decreased due to the hindered electron transfer of biomolecules. As shown in curve f, the CV response increased, due to the removal of DNA-Eu@MOF. When the Ag NPs was modified on the edge of TDNs, a new pair of symmetric redox peaks was observed in curve c, d, e, and f. The redox peaks were attributed to the Ag NPs, the anodic peak at 0.14 V represented the oxidation of Ag NPs to Ag_2O. These redox peaks further proved the presence of Ag NPs on the TDNs.

Optimization of the experimental conditions.

In order to obtain the best detection of MUC1, a series of conditions for this biosensor were optimized, including the concentration of the co-reactant $K_2S_2O_8$, the incubation time and temperature of DNA-Eu@MOF, the incubation time and temperature of MUC1. The concentration of co-reactant is an important factor. The ECL intensity increased with increasing $K_2S_2O_8$ concentration in the range of 0.04-0.14 M (Fig. S3A). The largest ECL intensity was significantly increased in the range of 0.04-0.1 M. When the concentration reached 0.12 M, the ECL intensity changes were not obvious. The $K_2S_2O_8$ concentration did not exceed 0.14 M due to solubility limitations. Hence, the optimal concentration was considered to be 0.12 M. As shown in Fig. S3B, the ECL intensity of the biosensor showed a clear trend with regard to incubation time, and the best incubation time of DNA-Eu@MOF was found to be 120 min. The ECL intensity was greatly affected by the incubation temperature of DNA-Eu@MOF (Fig. S3C). Low temperature conditions were not conducive to the modification of DNA-Eu@MOF on the electrode. Hence, the best incubation temperature was 37℃. In order to obtain excellent biosensor performance, the incubation time and temperature of MUC1 were crucial factors. The ECL biosensor response decreased with

increased incubation time in the range 30-50 min (Fig. S3D). After 50 min, the response may have been caused by non-specific adsorption. Therefore, 50 min was selected as the best incubation time. The effect of MUC1 incubation temperature on the biosensor resulted in slight fluctuations in the range of 30–40℃, but the lowest response was seen at 30℃ (Fig. S3E). Hence, the optimal temperature was considered to be 30℃.

Figure Captions

Figure S1. SEM image of Eu@MOF.

Figure S2 TEM image and the corresponding EDS mapping of Eu@MOF.

Figure S3. The EIS (A) and CV (B) for the stepwise biosensor fabrication (a) bare gold electrode, (b) TDNs/gold electrode, (c) Ag NPs/TDNs/gold electrode, (d) MCH/ Ag NPs/TDNs/gold electrode, (e) DNA-Eu@MOF/ MCH/ Ag NPs/TDNs/gold electrode, and (f) MUC1/ DNA-Eu@MOF/ MCH/ Ag NPs/TDNs/gold electrode.

Figure S4. Effects of (A) the concentration of $K_2S_2O_8$, (B) incubation time of DNA-Eu@MOF, (C) incubation temperature of DNA-Eu@MOF, (D) incubation time of MUC1, and (E) incubation temperature of MUC1.

Table Captions

Table S1. Comparison of various methods used for MUC1 detection.

Table S2. Detection of MUC1 added to human serum (n=3) using the proposed biosensor.

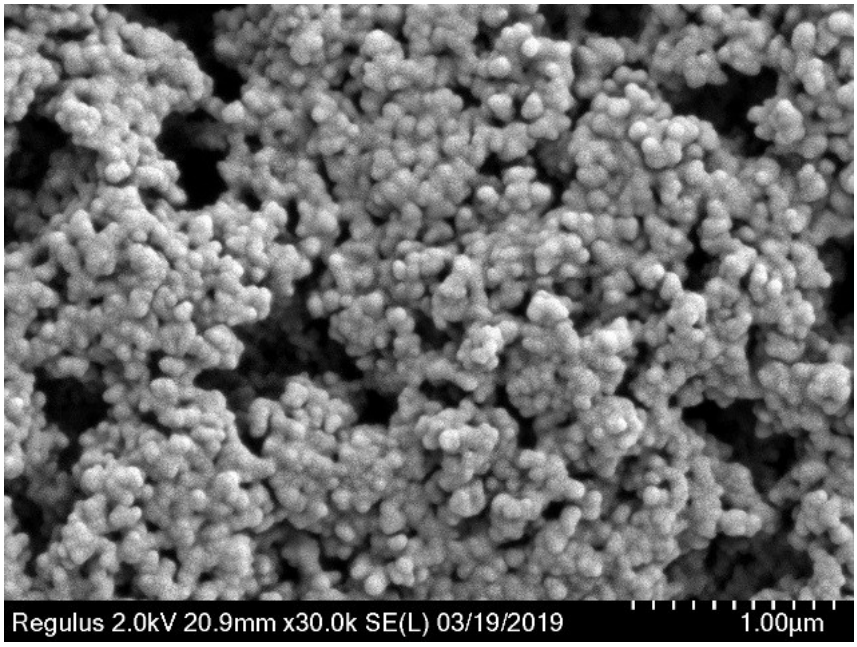

Figure S1

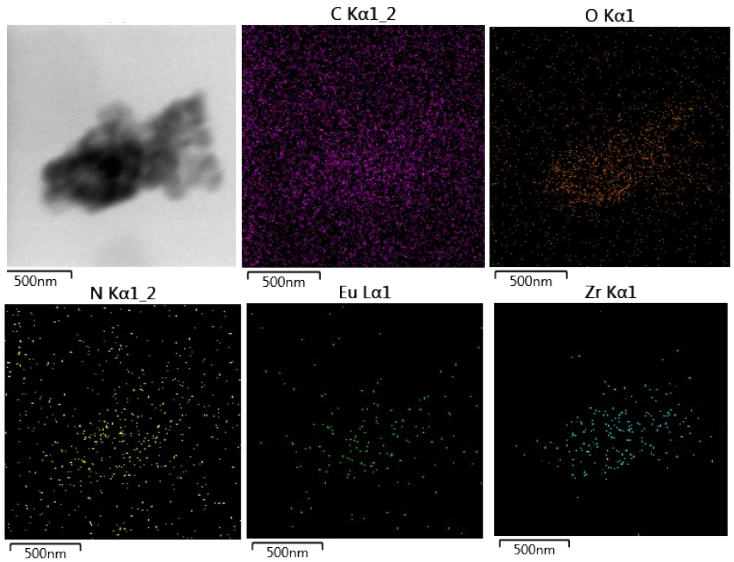
C Kα1_2
O Kα1
500nm
500nm
500nm
N Kα1_2
Eu Lα1
Zr Kα1
500nm
500nm
500nm

Figure S2

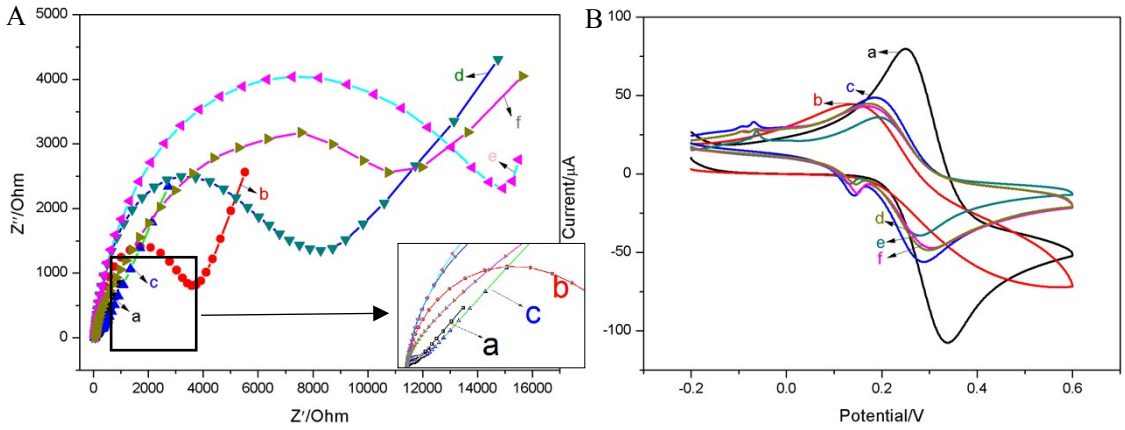

Figure S3

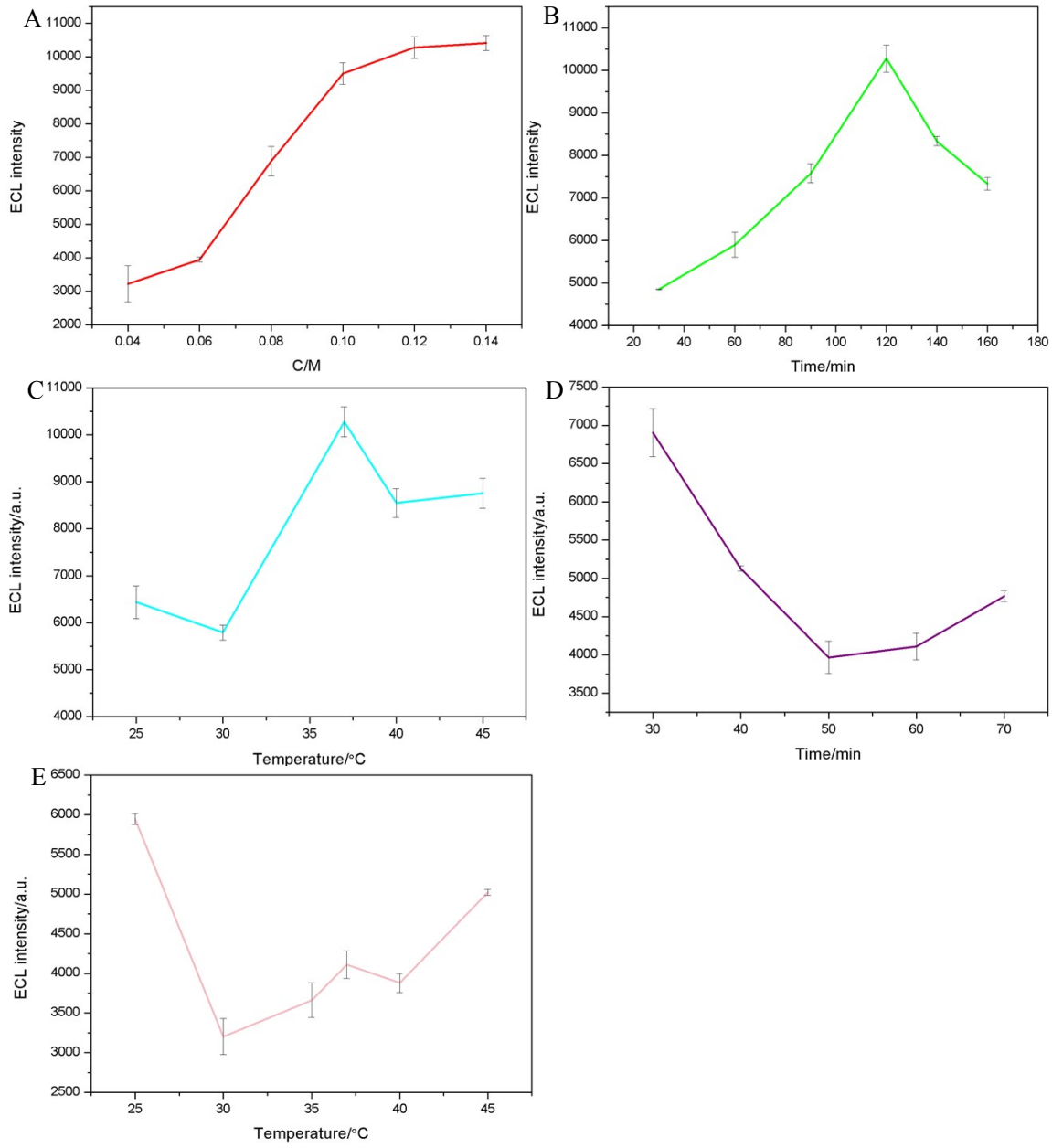
A
ECL intensity
C/M
B
ECL intensity
Time/min
C
ECL intensity/a.u.
Temperature/°C
D
ECL intensity/a.u.
Time/min
E
ECL intensity/a.u.
Temperature/°C

Figure S4

Table S1

Method	Detection range	Detection limit	Reference
EC	1 pM-1 μM	0.25 pM	1
SERS	10 fg/mL-100 ng/mL	10 fg/mL	2
FL	1 ng/mL-12 ng/mL	0.0748 ng/mL	3
FL	1 pg/mL-20 ng/mL	0.23 pg/mL	4
EC	1 pg/mL-50 ng/mL	0.4 pg/mL	5
ECL	1.135 fg/mL-0.1135 ng/mL	0.37 fg/mL	This work

Table S2

Serum sample	Added	Found	Recovery (%)	RSD (%)
1	0.1135 ng/mL	0.1130 ng/mL	99.56	1.31
2	1.135 pg/mL	1.1397 pg/mL	100.41	2.73
3	11.35 fg/mL	10.72 fg/mL	94.45	2.30

Reference

(1) S. H. Yang, F. F. Zhang, Q. L. Liang, Z. H. Wang, *Biosens. Bioelectron.* **2018**, 120, 85-92.

(2) K. K. Reza, J. Wang, R. Vaidyanathan, S. Dey, Y. L. Wang, *Small*, **2017**, 13, 1602902.

(3) H. B. Si, L. J. Wang, Q. L. Li, X. X. Li, B. Tang, *Chem. Commun.* **2018**, 54, 8277-8280.

(4) W. T. Yang, Y. Shen, D. Y. Zhang, W. J. Xu, *Chem. Commun.* **2018**, 54, 10195-10198.

(5) C. Y. Lin, H. X. Zheng, Y. Y. Huang, Z. L. Chen, F. Luo, J. Wang, L. H. Guo, B. Qin, Z. Y. Lin, H. H. Yang, *Biosens. Bioelectron.* **2018**, 117, 474-479.